JACS
JOURNAL OF THE AMERICAN CHEMICAL SOCIETY
Article
Cite This: J. Am. Chem. Soc. XXXX, XXX, XXX−XXX
pubs.acs.org/JACS

# Mapping Forbidden Emission to Structure in Self-Assembled Organic Nanoparticles

Daniel A. Hinton,[‡,†] James D. Ng,[‡,†] Jian Sun,[§] Stephen Lee,[∥] Semion K. Saikin,[⊥,▽] Jenna Logsdon,[#] David S. White,[†,¶] Angela N. Marquard,[†] Andrew C. Cavell,[†] Veronica K. Krasecki,[†] Kassandra A. Knapper,[†] Katherine M. Lupo,[†] Michael R. Wasielewski,[#] Alán Aspuru-Guzik,[⊥,⊗,□,⬡] Julie S. Biteen,[∥] Padma Gopalan,[†,§] and Randall H. Goldsmith*[,†]

[†]Department of Chemistry, University of Wisconsin−Madison, 1101 University Avenue, Madison, Wisconsin 53705, United States
[§]Department of Materials Science and Engineering, University of Wisconsin−Madison, Madison, Wisconsin 53706, United States
[∥]Department of Chemistry, University of Michigan, Ann Arbor, Michigan 48109-1055, United States
[⊥]Department of Chemistry and Chemical Biology, Harvard University, Cambridge, Massachusetts 02138, United States
[▽]Institute of Physics, Kazan Federal University, Kazan 420008, Russian Federation
[#]Department of Chemistry and Institute for Sustainability and Energy at Northwestern, Northwestern University, Evanston, Illinois 60208-3113, United States
[¶]Department of Neuroscience, University of Wisconsin−Madison, 1111 Highland Avenue, Madison, Wisconsin 53705, United States
[⊗]Biologically-Inspired Solar Energy Program, Canadian Institute for Advanced Research (CIFAR), Toronto, Ontario M5S 1M1, Canada
[□]Department of Chemistry and Department of Computer Science, University of Toronto, Toronto, Ontario M5S 3H6, Canada
[⬡]Vector Institute for Artificial Intelligence, Toronto, Ontario M5S 1M1, Canada

Supporting Information

**ABSTRACT:** The interplay between micromorphology and electronic properties is an important theme in organic electronic materials. Here, we show that a spirofluorene-functionalized boron-dipyrromethene (BODIPY) with an alkyl norbornyl tail self-assembles into nanoparticles with qualitatively different properties as compared to the polymerized species. Further, the nanoparticles exhibit a host of unique emissive properties, including photobrightening, a blue satellite peak, and spectral diffusion. Extensive photophysical characterization, including single-particle imaging and spectroscopy, and time-resolved fluorescence, coupled with electronic structure calculations based on an experimentally determined crystal structure, allow a mechanism to be developed. Specifically, BODIPY chromophores are observed to form quasi-two-dimensional layers, where stacking of unit cells adds either J-aggregate character or H-aggregate character depending on the direction of the stacking. Particularly strongly H-coupled domains show the rare process of emission from an upper exciton state, in violation of Kasha's rule, and result in the blue satellite peak. The spatial heterogeneity of structure thus maps onto a gradient of photophysical behavior as seen in single-particle imaging, and the temporal evolution of structure maps onto fluctuating emissive behavior, as seen in single-particle spectroscopy. Taken together, this system provides a striking example of how physical structure and electronic properties are intertwined, and a rare opportunity to use one to chart the other.

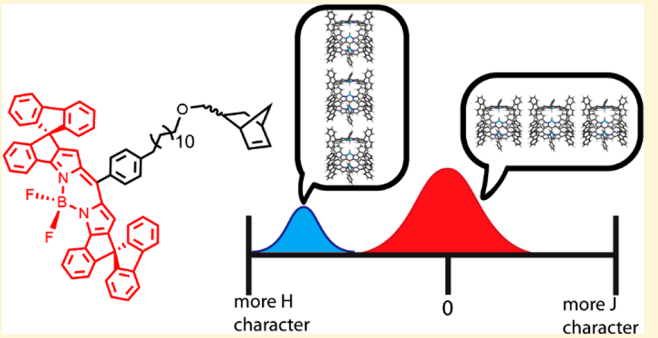


## INTRODUCTION

Synthetic multichromophore arrays are versatile nanoscale platforms for controlling and understanding the photophysics of exciton transport. A rich variety of emergent phenomena, including long-range energy transfer,[1,2] superradiance,[3] unusual scaling laws,[4] and exciton blockades[5,6] can be observed. Shifting from covalently organized scaffolds to self-assembled systems offers additional opportunities for emergent properties and applications,[7] but also reduces direct control. In particular, small changes in chemical structure may have dramatic effects on morphology, which in turn may have dramatic effects on

Received: August 24, 2018
Published: October 29, 2018






DOI: 10.1021/jacs.8b09149
J. Am. Chem. Soc. XXXX, XXX, XXX−XXX

photophysical behavior.[8,9] For example, with small interchromophore distances, balancing interaction strength with the opening of new quenching pathways can be difficult.[10] Similarly, when multiple electronic states are involved, small changes to energetics can result in fundamentally different relaxation and emission mechanisms. This article details the discovery and exploration of a self-assembled chromophore nanoparticle where specific structural motifs of domains within the nanoparticle map onto qualitatively different emissive properties, a rich example of the diversity that can emerge in self-assembled organic materials.

Applications of assembled organic nanomaterials that take advantage of these emergent phenomena range from fluorescence imaging[11,12] to organic optoelectronic devices[13,14] (OLEDs, OFETs, molecular electronics) to artificial photosynthesis.[15−17] In biomedical imaging applications, organic nanoparticles have higher *in vivo* compatibility as compared to inorganic nanomaterials.[11] In particular, nanoparticles composed of polymer-bound chromophores (Pdots)[12] have recently been shown to be effective imaging agents. Borondipyrromethene (BODIPY) chromophores incorporated into Pdots result in narrow-band emission, a useful feature for multiplexed imaging.[18] In that study,[18] the mole fraction of BODIPY monomers needed to be kept low to avoid self-quenching and spectral broadening, two undesirable aggregation-based processes and vivid examples of the balance required for optimizing properties. A variety of conjugated polymers which contain BODIPY dyes in the main chain have been synthesized and characterized.[19−21] However, polymer scaffolds also present disadvantages, including solubility constraints and difficulty of synthesis.

Here, we present organic nanoparticles derived from self-assembled BODIPY monomers, where the emergent behavior of the self-assembled particle deviates considerably from the polymerized sample. Most conspicuous is a significantly blue-shifted satellite emission peak. Nonuniformities in the brightness and emission spectrum across the particle suggest a nontrivial role of particle morphology. Self-assembled particles were also observed to brighten upon prolonged photoexcitation, a behavior seen in inorganic nanocrystals[22,23] but previously unobserved in organic nanoparticles. These behaviors were investigated by a combination of steady-state bulk spectroscopy, single-particle microscopy and spectroscopy, time-resolved bulk spectroscopy, structural characterizations, and via electronic structure calculations. Different emission patterns are shown to map onto different structural morphologies which offer different sets of allowed radiative transitions, including the rarely observed phenomenon of emission from an H-aggregated structure. Taken together, our experiments reveal how a simple molecule presents a uniquely rich array of photophysical phenomena, that can then be used to illustrate the dominant role of morphology. We expect these themes to be important in optimizing organic nanomaterials for their most promising applications.

## RESULTS

**Dye-Labeled Monomer and Polymer.** Our target chromophore is a spiro-conjugated BODIPY dye[24] that can be excited with a commercial 633 nm red laser. Using red excitation results in less background fluorescence due to impurities, a feature that has motivated use of this dye in recent single-molecule fluorescence microscopy experiments, where the dye was incorporated as a spectator-fluorophore for monitoring chemical dynamics of individual molecules.[25,26] This dye also offers the key feature of being rigid, yet nonplanar. We had expected this structural property to result in less aggregation, which is often a potential drawback of planar dyes.[27] We incorporated this chromophore into a polymeric scaffold by attaching it to a moiety which would undergo ring-opening metathesis polymerization (ROMP) (Figure 1). By selecting a fast-initiating catalyst, ROMP can be rendered living and, therefore, one can synthesize very well-defined, monodisperse polymers.[28]

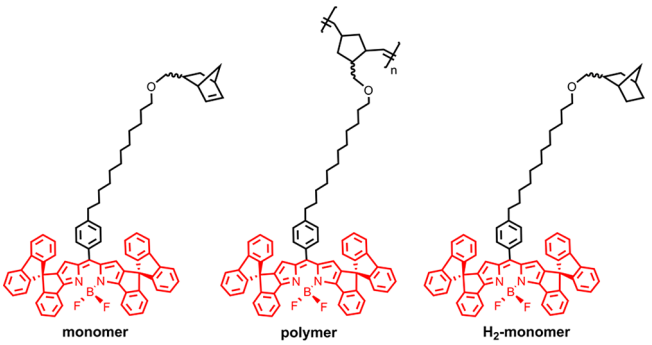


**Figure 1.** Structure of BODIPY-labeled fluorescent norbornene monomer, fluorescent norbornene polymer, and the hydrogenated monomer.

**Monomer Synthesis.** A common method for synthesizing BODIPY dyes combines an aldehyde and a pyrrole in a one-pot, multistep reaction.[29,30] The spiro-conjugated pyrrole was synthesized following published procedures.[24] An aldehyde functionalized with a norbornene unit and flexible alkyl chain was synthesized as per Figure 2. First, 1,4-dibromobenzene was reacted with *n*-butyllithium followed by addition of 1,12-dibromododecane to obtain compound **1** (Figure 2).[31] Next, an O-alkylation was performed to attach 5-norbornene-2-methanol followed by conversion of the aryl bromide **2** to the aryl aldehyde by treatment with *n*-butyllithium and then DMF. Aqueous workup provided aldehyde **3**.

The aldehyde and pyrrole were combined and treated with a catalytic amount of trifluoroacetic acid, followed by dichlorodicyanobenzoquinone (DDQ), then buffering triethylamine and boron trifluoride diethyl etherate to generate the desired BODIPY monomer **5** (Figure 1 and 2, **monomer**). The monomer was purified by column chromatography and characterized by $^{1}$H NMR, $^{13}$C NMR, high-resolution mass-spectrometry, and UV/vis spectroscopy. All synthetic details and characterization data can be found in the Supporting Information.

**Polymer Synthesis.** Grubbs Generation III catalyst was prepared by reacting Grubbs Generation II catalyst with 3-bromopyridine.[28] Fresh catalyst was then reacted with **monomer**, resulting in **polymer**, Figure 1, with $M_n$ = 22 240 Da (~22 monomer units, Table 1) as determined by GPC (Supporting Information).

**Solution Phase Absorption and Fluorescence.** The **monomer** and **polymer** have similar absorption spectra in toluene, with a $\lambda_{max}$ of 639 nm, and fluorescence emission from the monomer at 643 nm, with polymer emission 120 cm$^{-1}$ redder, at 648 nm (Figure 3a). In a 0.1% v/v solution of toluene/isopropyl alcohol (IPA), the **monomer** absorbance and fluorescence blueshift to 634 and 639 nm, respectively,


DOI: 10.1021/jacs.8b09149
J. Am. Chem. Soc. XXXX, XXX, XXX−XXX

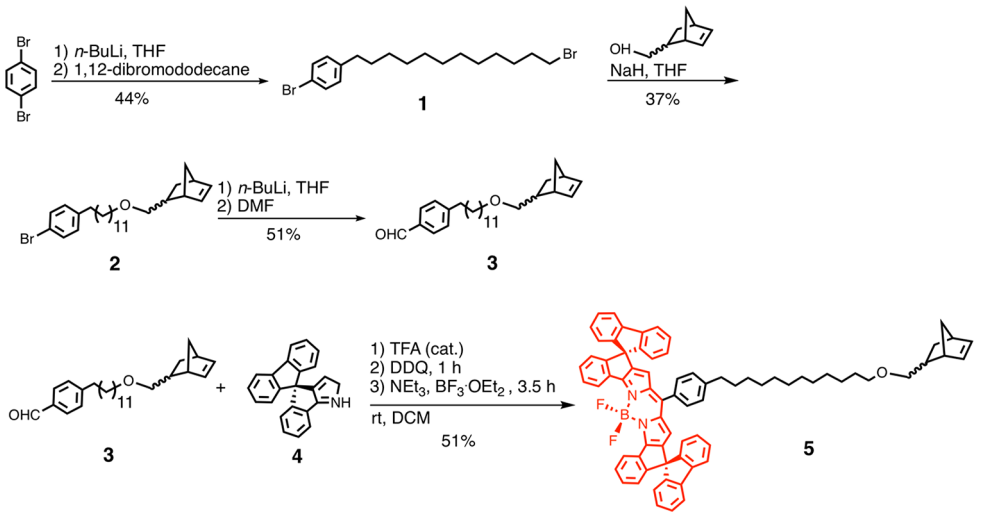


**Figure 2.** Reaction scheme for synthesis of monomer **5**.

**Table 1. Molecular Weight and Polydispersity of BODIPY-Norbornene Polymer**

| | |
|---|---|
| $M_n$ (Daltons) | 22,240 |
| $M_w$ (Daltons) | 38,270 |
| PDI = $M_w/M_n$ | 1.721 |

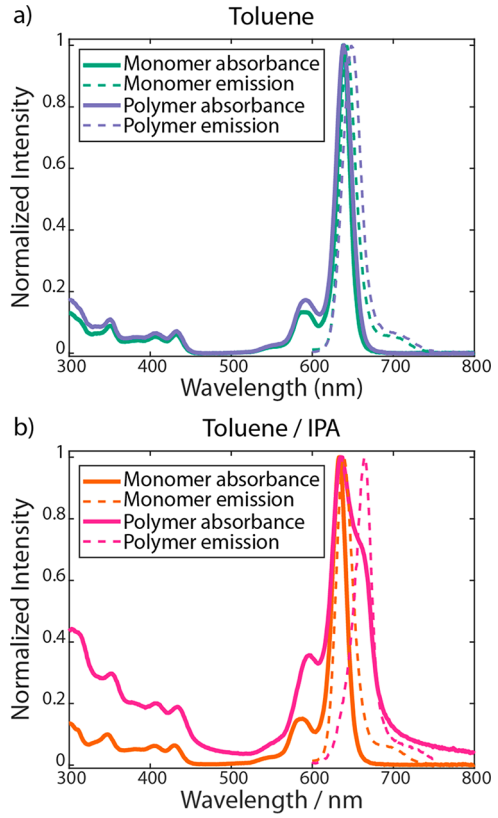


**Figure 3.** Absorbance and fluorescence emission spectra of BODIPY **monomer** and **polymer** in toluene (a) and 0.1% v/v toluene/IPA mixture (b). Absorbance and fluorescence are normalized to $\lambda_{max}$. Fluorescence excitation is at 580 nm. The **monomer** blueshifts slightly in the mixed solvent, while the **polymer** absorption broadens and redshifts.

while the **polymer** absorbance develops a red shoulder around 660 nm, with a fluorescence redshift to 665 nm (Figure 3b). The shoulder in the absorbance peak of the BODIPY-norbornene **polymer** in the toluene/IPA solution suggests aggregation of BODIPY units, with the overall red-shift likely indicating chromophores arranged in a J-stacked configuration, but the width of the peak suggests a variety of arrangements spanning H and J aggregates. However, the reduced quantum yield (Table 2) of the **polymer** in toluene/IPA suggests that

**Table 2. BODIPY Quantum Yields**

| | Monomer | Polymer |
|---|---|---|
| QY in Toluene | 0.55 ± 0.08 | 0.50 ± 0.07 |
| QY in 0.1% toluene in IPA | 0.5 ± 0.1 | 0.044 ± 0.003 |

there is facile energy transfer to traps that leads to a drastic quenching of the BODIPY fluorescence compared to the **monomer** in similar conditions.

**Single-Molecule and Single-Particle Microscopy.** Single-molecule spectroscopy and microscopy have a history of providing mechanistic insights into organic materials, including for conjugated polymers,[32−35] multichromophore systems,[5,36−38] and model systems for OLEDs.[39] 5 ng/mL solutions of **monomer** and **polymer** were spin-coated from toluene onto glass coverslips as well-separated nano-objects, Figure 4a. Monomers and polymers showed single-step photobleaching and blinking behavior, Figure 5a. While single-step bleaching is typical of individual fluorophores, such behavior in polymers suggests a well-coupled multi-chromophore system.[5,6,40] Further, even when polymer molecules are in their most emissive state, their intensities are comparable to the intensities exhibited by the monomers (Figure 5a), despite an average polymer size near 22 monomers. Thus, a potent quenching mechanism must be operative in order to not have increased brightness despite the increased number of fluorophores. Since the quantum yield of monomers and polymers in toluene is similar as determined via the solution-phase steady-state spectroscopy (Table 2), these quenching mechanisms are only operative in the single-particle measurement, either because of the absence of solvent, presence of the surface, or higher excitation intensities which may result in saturation effects.[4]



DOI: 10.1021/jacs.8b09149
J. Am. Chem. Soc. XXXX, XXX, XXX−XXX

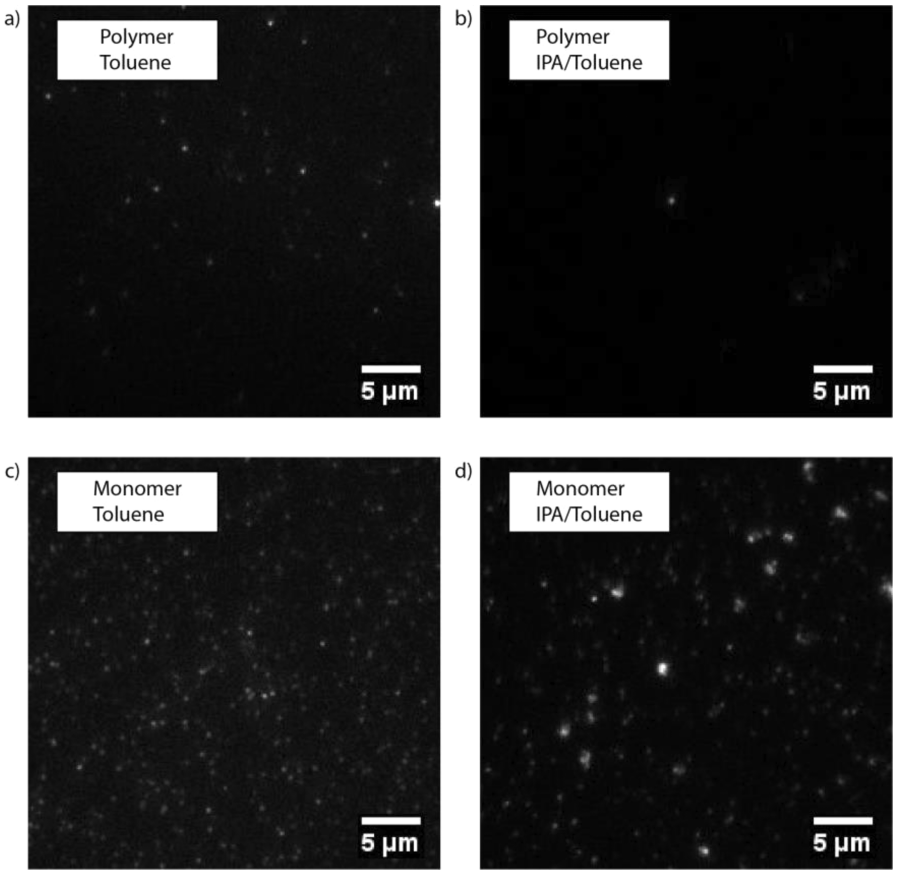


**Figure 4.** Samples of polymer and monomer spin-coated from 5 ng/mL solutions, excited at 633 nm at an intensity of 25 W/cm$^2$ and imaged with a 30 ms exposure time. Polymer spin-coated from toluene (a) and 0.1% v/v toluene/IPA (b) deposited as a sparse coating of particles of similar brightness. Monomer spin-coated toluene (c) deposited as a more densely populated layer, with similar brightness. Monomer deposited from 0.1% v/v toluene/IPA (d) densely covers the surface, and is significantly brighter. All images displayed with similar brightness and contrast.

A growing body of research has demonstrated the importance of solvents in shaping the morphology (and therefore, bulk properties) of organic materials including in individual conjugated polymer chains.[34,35,41−43] For instance, solvent vapor annealing (SVA) has been used as a postprocessing method to change film morphology, and these changes have been systematically examined at the single-polymer level.[35] Large differences in aggregation propensity were observed between solvent systems of disparate polarity.[35] For our work, in order to test the effect of changing the deposition solvent on our polymer photophysics, we made a 5 ng/mL solution of **polymer** in 0.1% vol/vol toluene/isopropanol (IPA) by diluting the toluene stock in IPA. The **polymer** samples spin-coated from the polar solvent mixture show discrete intensity levels of similar brightness to those spin-coated from pure toluene at this low concentration, but with a lower surface density (Figure 4a,b). While Table 2 reports quantum yields of similar value for **monomer** and **polymer** in toluene, in toluene/IPA the quantum yield of the **polymer** is significantly decreased, whereas the solution-phase **monomer** quantum yield is largely unaltered. Thus, whereas the quenching of the **polymer** relative to the **monomer** in toluene is not seen in solution and is only seen in the single-particle measurement, in toluene/IPA the **polymer** is quenched relative to the monomer in both solution and in the single-particle measurement, suggesting that quenching mechanisms, including formation of aggregates with H character, are operational in solution and at the surface.

Surprisingly, the monomer spin-coated at 5 ng/mL from a toluene/IPA mixture shows individual nano-objects with significantly increased fluorescence intensity compared to both the monomer deposited from toluene and the polymer deposited from toluene/IPA (Figure 5a). Emission from these nano-objects does not show blinking or single-step photobleaching, suggesting that monomers deposit as aggregates under these deposition conditions, and that the aggregation does not result in quenching, a sharp contrast to the behavior exhibited by the polymers that show emission intensity comparable to isolated monomers.

Increasing the deposition concentration of the toluene solutions of both monomer and polymer to 5 $\mu$g/mL increases the surface coverage, leading to the formation of a thin film (see Supporting Information). Depositing monomer from 0.1% v/v toluene/IPA solvent mixture at 5 $\mu$g/mL results in bright fluorescent particles which are still clearly spatially resolved, with surface densities comparable to the 5 ng/mL deposition condition (Figure 6b), but the individual particles are substantially brighter. Adjusting for different imaging conditions, these new particles are 400 times brighter than at the lower concentration (see Supporting Information). Polymers deposited from these conditions are also brighter (Figure 6a) and also show sustained emission without blinking or photobleaching (Figure 5b), in contrast to the more dilute deposition conditions where blinking was prevalent. However, polymer particles were still substantially dimmer than monomer particles.


DOI: 10.1021/jacs.8b09149
J. Am. Chem. Soc. XXXX, XXX, XXX−XXX

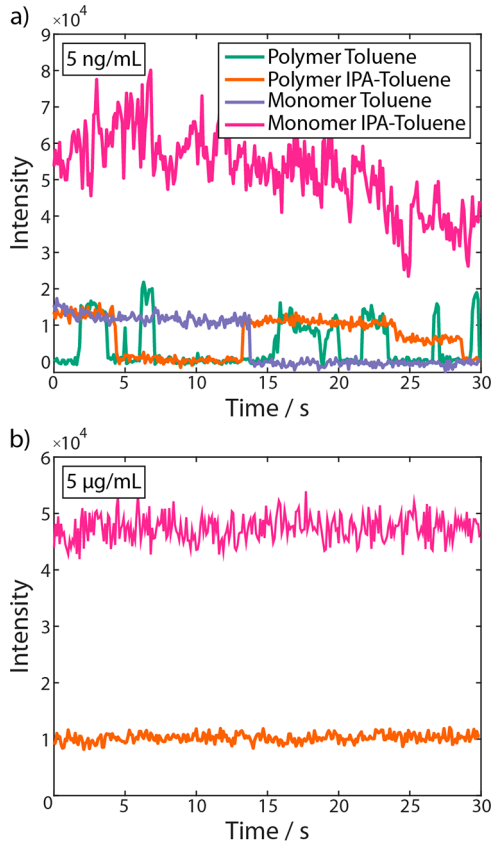


**Figure 5.** Single particle trajectories from 5 ng/mL videos (a) and 5 $\mu$g/mL videos (b) depicted in Figures 4 and 6. ng/mL traces taken at 28 W/cm$^2$, 30 ms exposure time. $\mu$g/mL traces taken at 280 mW/cm$^2$, 10 ms exposure time. At 5 ng/mL, particles blink, indicating fluorescence from a single or small number of molecules, and have similar brightness, under all conditions except for **monomer** spin-coated from 0.1% toluene/IPA. At 5 $\mu$g/mL, **monomer** nanoparticles act as a large number of emitters, without blinking.

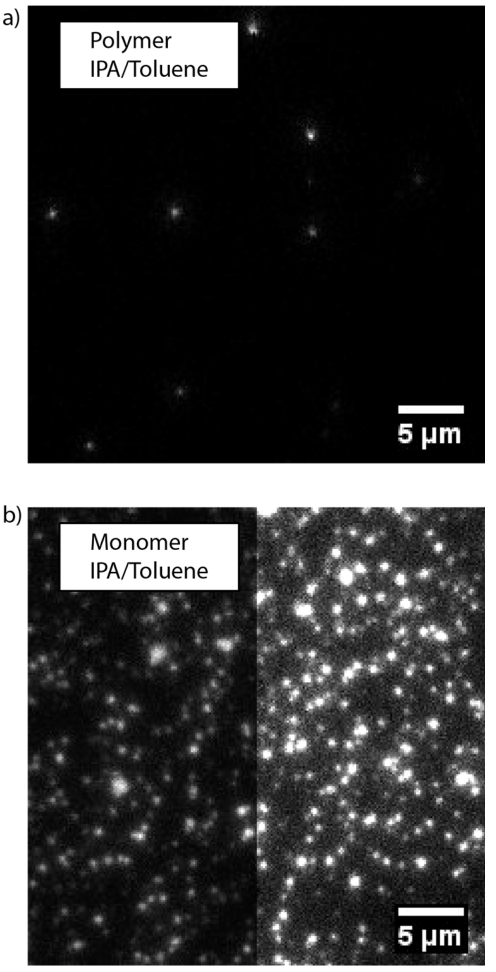


**Figure 6.** Samples of **polymer** and **monomer** spin-coated from 5 $\mu$g/mL solutions, excited at 633 nm at an intensity of 0.25 W/cm$^2$ and imaged with a 10 ms exposure time. **Polymer** deposited from 0.1% toluene/IPA still sparsely covers the surface (a), and **monomer** deposited from the mixed solvent (b) is still a dense layer of isolated spots, much brighter than samples prepared at 5 ng/mL. Panel b, right is displayed under similar brightness/contrast settings to panel a whereas panel b, left is rescaled to avoid saturation.

**Photobrightening.** When excited near their absorption maximum at 633 nm, the emission from bright aggregated **monomer** nanoparticles is largely constant over minutes, with slow photobleaching (Figure 7, red). However, when excited at 532 nm, surprisingly, the aggregated **monomer** nanoparticles show increasing fluorescence intensity over time (Figure 7, light green and dark green). Fluorescence intensity of particles spin-coated at 6 $\mu$g/mL increased by over 250% over 500 s when excited at high excitation intensity (Figure 7, dark green), before eventually photobleaching. While the degree of brightening was variable, increasing emission over time was consistently observed. **Polymer** samples under similar conditions exhibited the typically observed slow photobleaching, without the period of increasing fluorescence (Supporting Information), indicating that the photobrightening behavior is unique to the aggregated **monomer**.

Photobrightening with excitation at 532 nm can occur if a population is being irreversibly converted to a new photoproduct with stronger 532 nm absorption and emission, which would result in decreased emission from the original red species. To test for this possibility, we used alternating excitation between 532 and 640 nm light (Figure 7, dashed red and green) with emission spectrally resolved into two channels separated by a 650 nm dichroic mirror. Though the brightening was uniquely driven by excitation at 532 nm light, the emission intensity increased whether the sample was excited by green or red light, contradicting the hypothesis of a new photoproduct described above. To better understand these unexpected photophysics, we further characterized particles formed from **monomer** deposited at 5–6 $\mu$g/mL. All further characterization was applied to these high-concentration monomer-derived nanoparticles unless otherwise mentioned.

**Single-Particle Spectroscopy.** To further explore the physical transition that occurs during photobrightening, emission spectra of single particles were acquired as a function of time. Single-particle spectra of one representative **monomer** nanoparticle excited at 532 nm shows a broad peak centered at 650 nm likely originating from $S_1$ emission, with an unexpected blue satellite peak which blinks on and off and diffuses spectrally, ranging from 550 to 600 nm, Figure 8. A trivial source of dual emission could be the presence of a fluorescent impurity in the **monomer**. However, an excitation spectrum of **monomer** in solution measuring emission at the emission maximum contains all the absorption features of the solution spectrum, ruling out a chemical impurity (see Supporting


DOI: 10.1021/jacs.8b09149
J. Am. Chem. Soc. XXXX, XXX, XXX−XXX

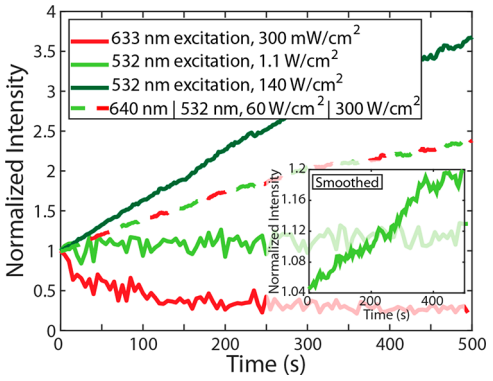


**Figure 7.** Fluorescence intensity trajectories of monomer particles excited at 633 nm (red) and 532 nm (greens). The particles increase in fluorescence intensity by more than 250% over 500 s when they are excited by green light at 140 W/cm$^2$ (dark green), and more subtly when excited with 1 W/cm$^2$ (light green) but bleach normally when excited by red light at 0.3 W/cm$^2$ (red). When alternately excited at 532 and 640 nm, the emission from 640 nm excitation increased over time instead of bleaching (red/green dashed trace). Smoothing and rescaling of the 532 nm, 1.1 W/cm$^2$ trajectory highlights the subtle increase in intensity over time (inset, light green).

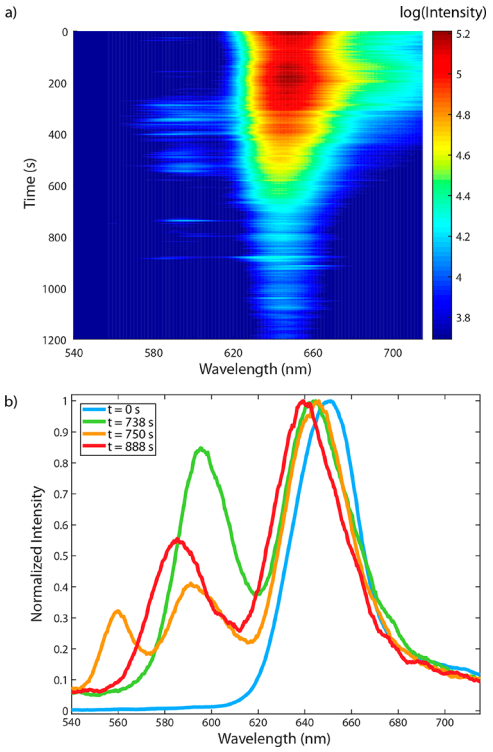


**Figure 8.** Spectra of a single monomer particle spin-coated from toluene−IPA mixture over time (a), and selected normalized spectra at several time points chosen to highlight emission from the blue satellite (b). The monomer nanoparticle shows an increase in fluorescence intensity before bleaching. Spectrally, the $S_1$ emission near 640 nm blue-shifts a small amount over time, and the relative intensity of the satellite peak increases largely due to bleaching of $S_1$ fluorescence after ∼700 s. The wavelength of the blue satellite is mostly centered at 590 nm (green), but occasionally spontaneously shifts to 580 nm (red), and extremely rarely displays a third even higher energy peak (orange). Spectra are smoothed with a moving mean of width ∼7 nm. CW excitation is provided at 532 nm at 690 W/cm$^2$.

Information). The major and minor solution-phase absorption and emission peaks do not follow the mirror image relationship expected of a vibronic progression, and the minor fluorescence peak is higher in energy than the major solution-phase absorption peak. Therefore, an additional mechanism that allows for radiation from higher electronic or excitonic species must be at play, in violation of Kasha's rule.[10]

**Spectrally Resolved Imaging.** Seeing the above evidence of spectral heterogeneity, we added a degree of spectral decomposition to our single-particle imaging by resolving the image into blue (560−590 nm) and red (660−720 nm) emission channels (Figure 9). When imaging small particles, no significant spatial differences were seen in the two color channels (though blue satellite emission was weaker as expected, see Supporting Information), likely to due to the subdiffraction limited particle size. However, spectrally decomposed imaging when applied to large (∼1 $\mu$m) particles showed a qualitatively different behavior. Surprisingly, while the red-channel emission from large **monomer** particles took the commonly observed form of homogeneous circular puncta (spots), emission in the spectral channel that includes the blue satellite appears as rings of fluorescence, Figure 9a. Prolonged excitation at 532 nm results in a collapse of the ring to a circular punctum, easily visible in sequential images (Figure 10a) or movies (see Supporting Information). Observation of rings only occurred in large aggregates, with the size of the aggregate depending sensitively on the deposition conditions including sample concentration and sample history. In contrast, the observation of photobrightening (Figure 7) was very robust to various sample preparation conditions.

## DISCUSSION

Norbornene functionalized BODIPY **monomer** and **polymer** were synthesized and compared. **Polymer** showed significant quenching in solution due to the close proximity of the pendant BODIPYs. The **monomer**, when spin-coated from a poor polar solvent mixture forms nanoparticles. Surprisingly, bright **monomer** nanoparticles fluoresce with increasing intensity as they are excited at 532 nm, and exhibit a blue satellite peak at 550−600 nm in addition to the typical $S_1$ emission near 650 nm, in violation of Kasha's rule. For large particles, the blue satellite peak occurs uniquely at the exterior rim of the particle while being absent at the particle centers, with a shifting spatial distribution over time. The intensity, spectral, and spatial changes in emission over time suggest a change in chemical structure or morphology of the nanoparticle aggregate.

Most organic fluorophores will eventually become oxidized to a nonfluorescent state after repeated photoexcitation, with a large collection of noninteracting fluorophores displaying an analog decrease in fluorescence intensity. Alternatively, emission can be increased over time if that emission is initially partially quenched by an energy acceptor that is subsequently eliminated. Indeed, increasing Förster resonance energy transfer (FRET) donor emission has been observed in FRET microscopy due to bleaching of an acceptor dye.[44,45] PbS[22] and CdSe[23] quantum dots have also been shown to brighten controllably under irradiation in a process due to filling of surface electron-trap sites. The validity of these mechanisms and others will be considered below for our system.

**Ruling out a Chemical Mechanism.** Nanoparticle photobrightening could derive from a chemical reaction, such as the result of an intra- or intermolecular photo-


DOI: 10.1021/jacs.8b09149
J. Am. Chem. Soc. XXXX, XXX, XXX−XXX

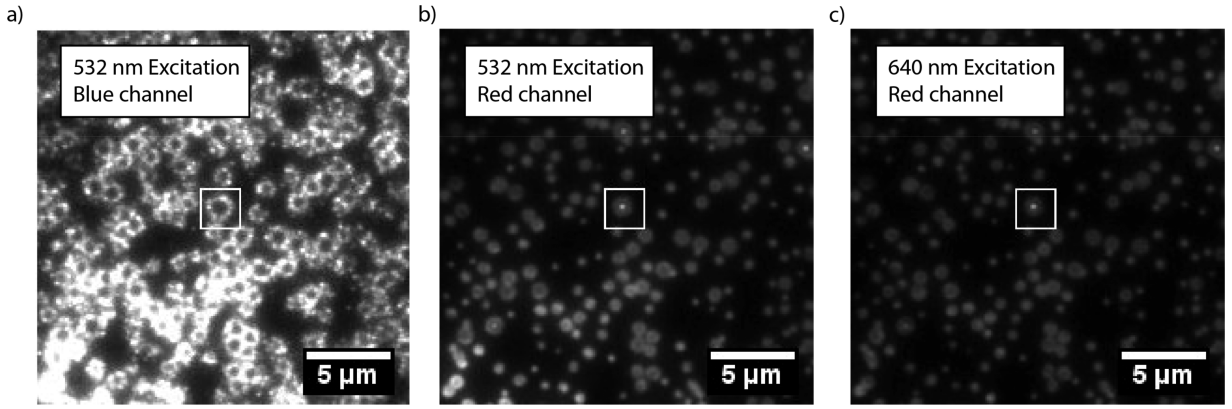


**Figure 9.** Images of large particles spectrally decomposed into blue (a, 560−590 nm) and red (b and c, 660−720 nm) channels with 532 nm excitation (a and b), or 640 nm excitation (c). All images set to the same brightness and contrast settings. Samples were excited at an intensity of 300 W/cm$^2$ at 532 nm, and 60 W/cm$^2$ at 640 nm. The particle used in Figure 10 is boxed in the center of the images.

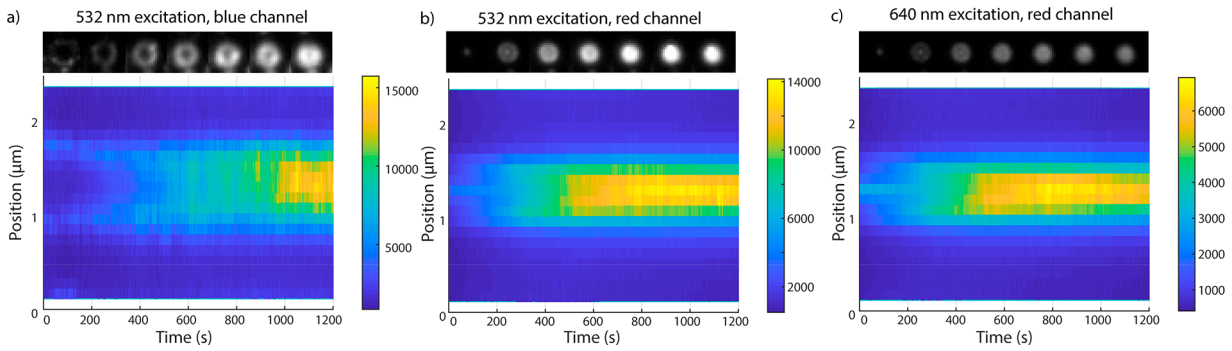


**Figure 10.** Waterfall plots of large monomer nanoparticle emission intensity under alternating excitation. Single monomer particle excited by alternating 532 nm (a,b) and 640 nm (c) laser light shows increasing fluorescence intensity in both the blue (a, 560−590 nm) and red (b, c, 660−720 nm) channels. Plots show fluorescence intensity of a line profile through a single particle ($y$) over time ($x$), with 2 s resolution. Over time, the particles become brighter in all channels, while remaining a similar size. The blue channel signal with 532 nm excitation shows initial fluorescence from a ring around the perimeter of the particle, which becomes more intense and fills in the center of the particle over time (a). Red channel fluorescence is concentrated inside the blue-channel fluorescent ring, is similarly localized in both excitation channels, and also increases over time.

cycloaddition reaction involving the norbornene alkene moiety and the BODIPY. The double bond in the strained ring system of norbornene is well-known for its high reactivity.[46,47] Additionally, norbornene is known to participate in visible light-mediated photocycloaddition reactions under mild conditions.[48] A new chemical species produced from such a reaction could have different photophysical properties and, therefore, be responsible for the observed photobrightening behavior. In order to rule this out, we hydrogenated the BODIPY monomer using palladium on carbon and hydrogen at atmospheric pressure yielding **$H_2$-monomer**, (Figure 1). **$H_2$-monomer** displayed the same behavior as the parent monomer when analyzed at the single-particle level (see Supporting Information). Therefore, we can confidently rule out any chemical behavior due to alkene reactivity of the norbornene moiety. The norbornene/norbornane moiety appears to function primarily as a morphology-directing group.

**Photobrightening Results from a Photothermal Mechanism.** Photobrightening only occurred upon excitation at 532 nm, while excitation at 633 nm produced continuous emission at a slowly decreasing intensity due to photobleaching, Figure 7. While excitation with higher energy 532 nm photons could access a higher electronic or vibronic state with a different photophysical fate, it much more commonly results in the same emission with a larger fraction of the input energy dissipated as heat (Kasha's Rule). That dissipated heat could result in morphological changes that could affect the apparent brightness. However, if a photothermal mechanism is responsible, external heating should also have an effect on emission properties. Heating spin-coated **monomer** nanoparticle samples on a hot plate at 80 °C led to an increased initial fluorescence intensity (see Supporting Information) and an absence of photobrightening after thermal annealing (Figure 11). The fluorescence intensity integrated over 200 s increases by a factor of 5 after 3 h of heating (see Supporting Information). After heating, the photobrightening effect vanishes, Figure 11. Because the photobrightening effects are mimicked by thermal annealing, the increased fluorescence over time is likely due to a photothermal mechanism, such as evaporation of solvent or thermal rearrangements of the dye molecules, leading to changes in the internal structure of the particles.

**Assessing Structure and Morphology of Nanoparticles.** Before delving into the unique optical phenomena, it is desirable to learn more about the dimensions and molecular packing of the self-assembled dye aggregates.

Atomic Force Microscopy (AFM) images were acquired (see Supporting Information). **Monomer** spin-coated onto glass from a 5 $\mu$g/mL 0.1% toluene/IPA mixture shows aggregation into well-separated nanoparticles 160 ± 30 nm in diameter and 14 ± 5 nm tall, with a surface density of 0.3 ±


DOI: 10.1021/jacs.8b09149
J. Am. Chem. Soc. XXXX, XXX, XXX−XXX

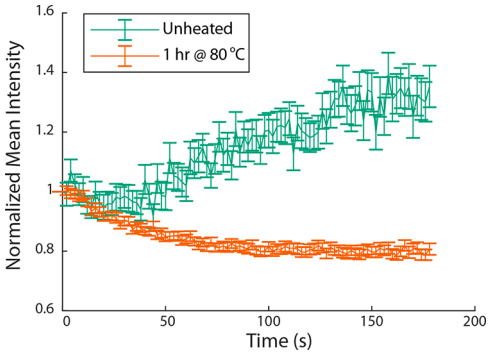


**Figure 11.** Summed intensity trajectories of many monomer nanoparticles upon 532 nm excitation as spin-coated (green) or after being preheated at 80 °C for 1 h (orange), normalized to initial intensity. Preheated samples are brighter (see Supporting Information) and do not continue to photobrighten, suggesting that the brightening mechanism is photothermal in nature.

$0.1/\mu m^2$. These conditions produce particles similar to those in Figure 6 as opposed to Figure 9.

To obtain more insight into the relative orientation of the BODIPY chromophores in the aggregates as directed by the norbornene tail, crystals of monomer were grown via slow diffusion ($CHCl_3/CH_3CN$) at room temperature for 72 h. The single-crystal X-ray diffraction (XRD) data was suitable for drawing basic conclusions regarding the relative orientation of the **monomer** BODIPY moieties (Figure 12), but not well-resolved enough to locate atoms within the alkyl chain or determine exact bond lengths and distances. The N−N vector within each BODIPY core is approximately parallel to the *a* axis, Figure 12a. The BODIPY units form corrugated sheets parallel to the *ac* plane, Figure 12b. These ∼18.7 Å thick layers are separated along the *b* axis by ∼27.8 Å (roughly the length of the extended alkyl chain). We suspect that these alkyl chains are extending along the *b* axis between the BODIPY layers. Likely, the BODIPY core units have a propensity to stack with one another into a somewhat organized structure largely due to solvent interactions while the long alkyl chains remain highly disordered. The balance between $\pi$ stacking interactions, steric repulsions from the spirofluorene groups, and segregation of disordered aliphatic chains is likely responsible for the quasi-two-dimensional BODIPY packing.

**Coupling between Morphology and Electronic Structure.** The crystal structure presented in Figure 12 provides a basis to formulate a model for the electronic structure of BODIPY aggregates that underlies the rich set of optical measurements presented above.

Simulated spectra of molecular aggregates were prepared as follows. First, electronic excitation spectra, transition dipoles, and transition densities of single BODIPY molecules were calculated using time-dependent density functional theory (Supporting Information). The lowest optically allowed electronic excitation is at 2.34 eV (530 nm) with the corresponding transition dipole about 10 D. The second optically active transition is at 3.4 eV (360 nm), which leaves an optically "dark" window of about 1 eV and allows consideration of only the lowest intramolecular transitions in the formation of collective excitonic states in the BODIPY aggregates. The collective excitonic states in the molecular aggregates are formed due to the Förster interaction between intramolecular excitations.[49] Frequently, to reduce the computational cost, this interaction is modeled using a multipole fit to microscopic models.[50] Here, we follow a different route and compute the intermolecular couplings directly from the transition densities. Spectra of small BODIPY aggregates are singly or doubly peaked with spectral position and density of states (DOS) highly sensitive to the shape of the aggregate, Figure 13.

Thus, the unit cell is an H-aggregate with a dipole-allowed upper exciton band shifted 400 $cm^{-1}$ blue of the isolated monomer while dipole forbidden states exist around −200 and −250 $cm^{-1}$, and thus there is a 650 $cm^{-1}$ splitting between the dipole allowed state and the next lowest state, Figure 13a. However, the nature of the interaction of the unit cell with other unit cells varies significantly depending on crystallographic orientation. As shown in Figure 12b, the BODIPY cores assemble in quasi-two-dimensional layers, with aliphatic chains largely insulating the BODIPY layers from each other. Figure 13b−d shows how the exciton coupling varies as unit cells are expanded along the remaining two crystallographic axes. Expansion along the *c* axis (Figure 13b) results in an additional blue shift, resulting in even more H character and a splitting between upper and lower exciton bands near 1000 $cm^{-1}$ for a trimer. In contrast, expansion along the *a* axis (Figure 13c) results in red shift, opposing the H character within the unit cell, resulting in a net J aggregate character.

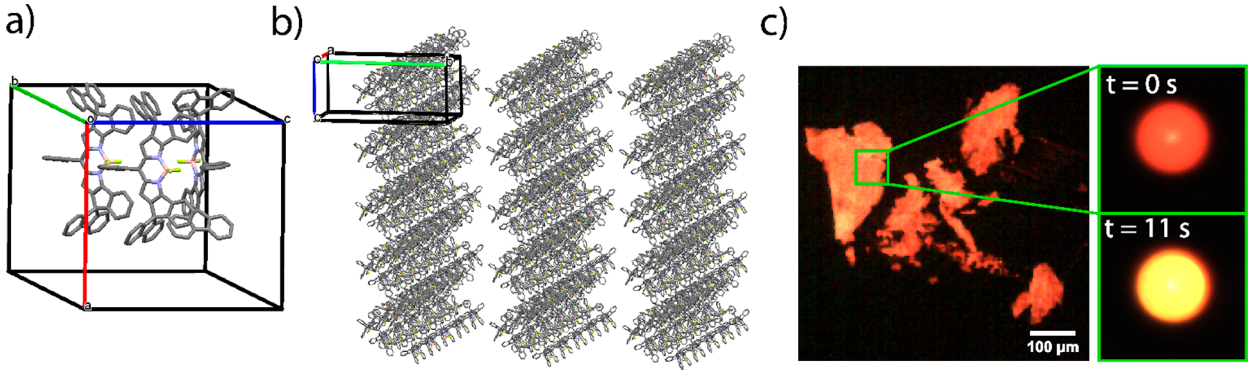


**Figure 12.** (a) View of the unit cell, showing three symmetry-independent BODIPY molecules, with cores oriented so that the N−N vectors are approximately parallel to the *a* axis. Color scheme: gray C, blue N, orange B, green F. (b) A molecular packing diagram illustrating the existence of quasi-two-dimensional sheets. Alkyl chains are not shown. (c) Individual crystals fluoresce red upon widefield excitation. Upon prolonged excitated with a more focused beam (diameter ∼ 150 $\mu$m), intense red emission is observed, followed by yellow emission (insets).


DOI: 10.1021/jacs.8b09149
J. Am. Chem. Soc. XXXX, XXX, XXX−XXX

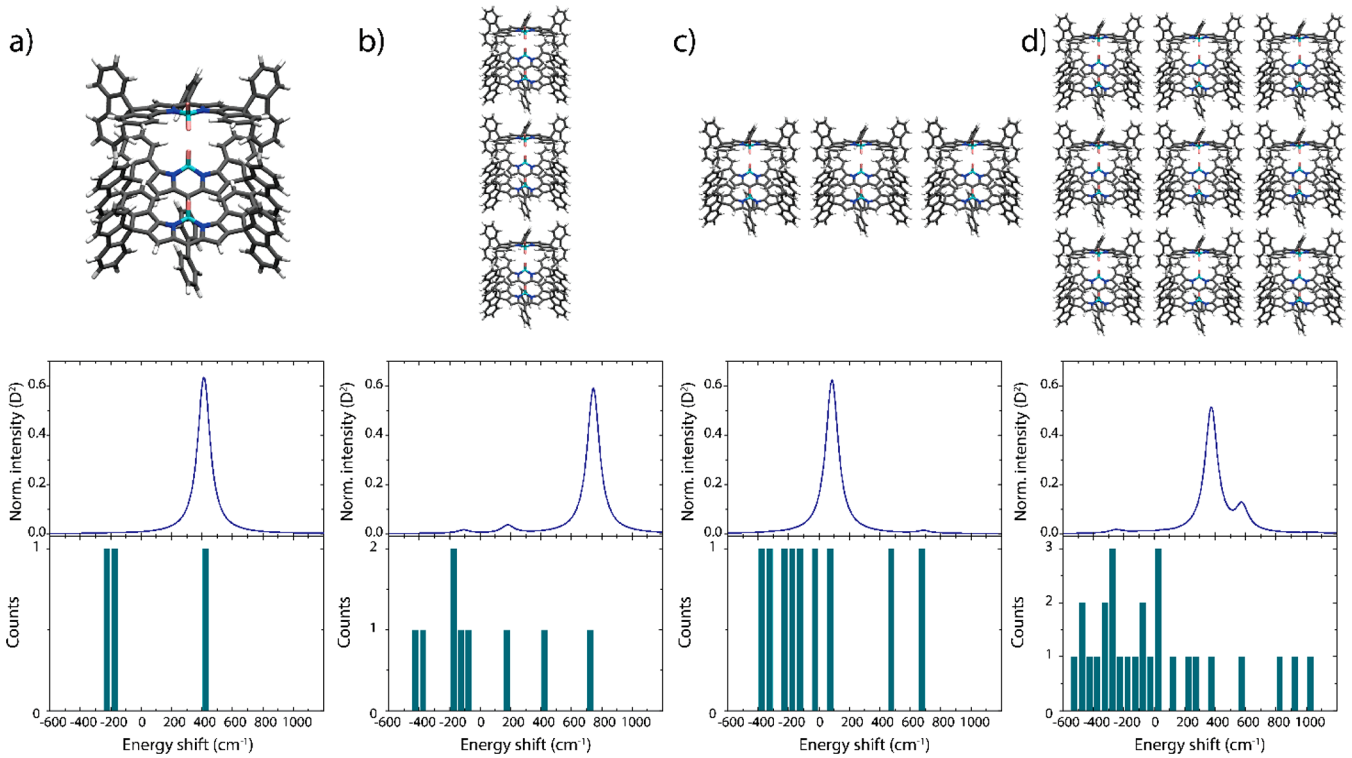


**Figure 13.** Correlation between unit cell packing (top), predicted spectra (middle) and density of states (DOS, bottom) for (a) a single unit cell, (b) a 1 × 3 unit cell aggregate, (c) a 3 × 1 unit cell aggregate, and (d) a 3 × 3 unit cell aggregate of **monomer**.

Creation of a full two-dimensional layer, Figure 13d, results in a dominant dipole-allowed transition net negligibly shifted from the isolated monomer, suggesting that interactions in the two crystallographic directions largely oppose each other in the ideal geometry. Extension of this effect to higher order aggregates, Figure 14, shows a saturation of the effect by ten unit cell repeats, with one-dimensional structures along the *c* axis showing a splitting between upper and lower exciton bands just exceeding 1000 $cm^{-1}$.

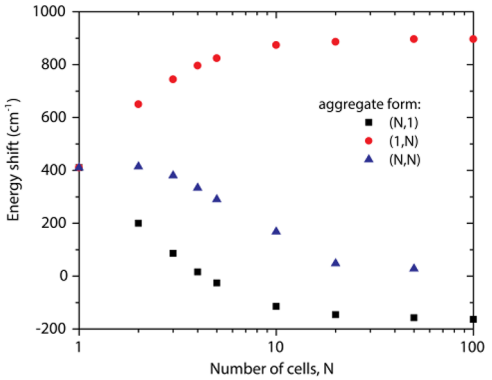


**Figure 14.** Energy shift of emissive band relative to the isolated monomer in 1D (black and red) and 2D (blue) aggregates of increasing number of unit cells (N). The (1,3) data point corresponds with Figure 13b and the (3,1) data point corresponds with Figure 13c.

This ideal geometry does not include the significant amount of disorder present in the aggregates, though it does provide a mechanism for how the geometry of different shaped nanodomains maps onto electronic structure. The smallest domains likely resemble a single or small number of unit cells, and thus a net H-character domain. Domains with eccentricity along one direction are then predicted to range from having strong H-character to weak J-character. Thus, fracturing the ideal two-dimensional array into nanodomains predicts a heterogeneous mixture of electronic state distributions, Figure 15a.

It is also important to emphasize that the single crystal structure is one of many possible geometries that may exist in the nanoparticle. For example, films made via dropcasting that are suitable for thin-film XRD show broad features (see

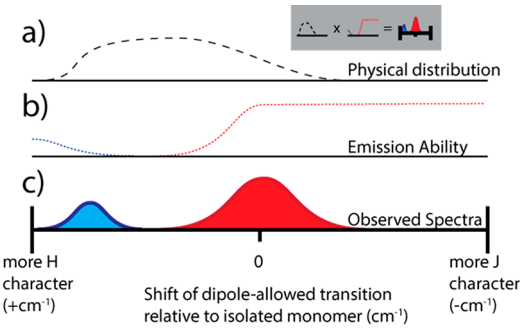


**Figure 15.** Summary of expected emissive properties. (a) Samples of monomer aggregates display a range of exciton coupling behaviors, ranging from weak J-aggregates to strong H-aggregates. (b) J-aggregates are expected to demonstrate red emission slightly or significantly red-shifted from the unaggregated monomer depending on the strength of the J-coupling. In contrast, weakly H-aggregated species should be nonemissive, and strongly coupled H-aggregates may display weak blue-shifted emission. (c) Taking into consideration the expected distribution of electronic structures and different emissive behaviors, this model predicts a major peak near the unaggregated monomer and a weaker blue satellite peak, as observed.


DOI: 10.1021/jacs.8b09149
J. Am. Chem. Soc. XXXX, XXX, XXX−XXX

Supporting Information) indicative of many contributing structures. These films do not show evidence of photobrightening or satellite emission, suggesting that the special geometries required for these phenomena exist in the nanoparticles but not in the thin film. On the other hand, the individual crystals used for the crystal structure shown in Figure 12a show photophysical behavior qualitatively similar to the nanoparticles. Upon illumination at 532 nm, individual crystals first show red emission but then show yellow emission (~560−590 nm) upon prolonged excitation, Figure 12c. Thus, molecules packed in this geometry also show the appearance of a blue-shifted spectral feature, suggesting that it is reasonable to use the determined crystal structure to understand the behavior of the nanoparticles. Photobrightening was also observed, but inconsistently as photobleaching was also quite rapid. Importantly, even as the crystal structure can provide a basis for the photophysical observations in the nanoparticles, it should be taken as one piece of evidence that a particular molecular ordering motif exists that can provide both H- and J-character. Other molecular packing geometries are also possible.

**Mapping Electronic Structure onto Emissive Properties and Time-Resolved Emission.** The final piece then is using the model of electronic structure above to predict emission behavior, Figure 16. Strongly J-coupled aggregates are expected to result in red-shifted fluorescence enhanced in intensity due to a transition dipole distributed across multiple molecules (i.e., superradiance).[51] However, as predicted above, due to the H-coupling within the unit cell, even the most favorable assemblies for generating J-coupling should only result in a weakly J-coupled aggregate, suggesting such strong red-shifted emission should not be seen, as is born out in experiments, Figure 8.

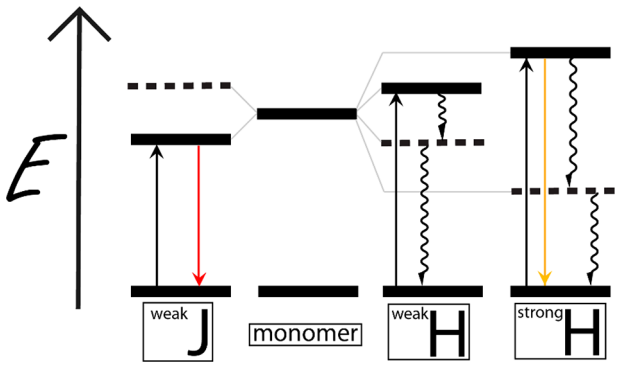


**Figure 16.** Jablonski diagram, showing emissive properties of observed aggregates. Weakly J-coupled aggregates are expected to demonstrate red emission, similar to the solution-phase monomer. Weakly H-coupled aggregates are expected to be nonemissive due to rapid internal conversion to the nonemissive lower exciton level. Strongly H-coupled aggregates will possess a large energetic splitting between the upper and lower exciton bands that will slow internal conversion, allowing weak emission from the upper exciton state, observable as emitted orange (near 580 nm) light, which is referred to as the "blue satellite" peak.

Weakly H- or J-coupled species should present with emission that is similar to the isolated monomer. The diagnostic feature of a distribution of weakly exciton-coupled species should be a broad emission peak centered close to the isolated monomer emission, as seen in experiments, Figure 8.

The most exotic observation in our experiments is the blue-shifted satellite peaks, Figure 8. H-aggregates result in blue-shifted dipole-allowed transitions, but are generally assumed to be nonemissive and at the heart of so-called "self-quenching" behavior. The origin of the quenching in H-aggregates is that rapid internal conversion from the upper dipole-allowed exciton level to the lower dipole-forbidden levels depopulates the radiative species, resulting in the population of formally nonradiative species that ultimately relax by further internal conversion to the ground state, Figure 16.[10] Thus, a dipole-allowed transition typically populates the upper exciton level (resulting in the characteristic blue shift of the absorption peak), but radiation from this state is outcompeted by internal conversion to a lower nonradiative state.

Although optical transitions from the lower excited state of a perfectly ordered H-aggregate is forbidden, there is precedent for emission from H-aggregates. Spano and Silva modeled the electronic states giving rise to emission from conductive polymers as HJ-aggregates, with J-like interaction between chromophores within polymer chains and H-like interaction across chains.[52] The diversity of polymer morphologies leads to a complex range of delocalized electronic states observed in different systems. Of note, regioregular poly(3-hexylthiophene) films emit from an entirely H-like state.[53,54] Emissive H-aggregates have also been observed in a number of small organic molecules. The mechanism generally involves imperfect H-aggregate formation, where angular rotation[55−58] or slip-stacking[59] between fluorophores leads to weakly allowed emission from the lower H-aggregate excited state. Alternatively, aggregation induced emission can occur when steric deactivation of isomerization or rotation reduces the nonradiative relaxation rate from the lower excited state.[55,60−63] In all of the cases of H-aggregate emission, emission was observed from the normally dark lower exciton-coupled state of the H-aggregate, and was thus red-shifted relative to the nonaggregated chromophore. Recently, Bayda and co-workers examined H-aggregates of phthalocyanines and observed emission from the upper exciton-coupled state.[64] They suggested that emission from the upper-exciton-coupled state was caused by thermal repopulation from the lower exciton-coupled state.[64] In all of these cases, H-aggregate emission, when observed, displayed a longer radiative lifetime than in the unaggregated chromophore. In all cases except for that reported by Bayda,[64] emission from the lower H-aggregate exciton peak is also red-shifted relative to unaggregated chromophore, unlike the blue satellite peak in our system.

To account for our blue satellite peak, we propose a different mechanism for emission from the H-aggregate, Figure 16. As described above, the first step of the quenching mechanism of the H-aggregate is internal conversion depopulating the upper species. However, the rate of internal conversion scales inversely with the energetic distance between the upper state and the lower states, resulting in the well-known "energy gap law" for estimating relative rates of internal conversion.[10] The prediction then is that strongly coupled H aggregates where a large energy gap exists should exhibit slower internal conversion that is less able to outcompete fluorescence. This behavior is seen in species with large energetic gaps between $S_1$ and $S_2$ electronic states.[65] For example, room temperature solutions of 1,4-anthraquinone show emission from both $S_1$ and $S_2$ states with an 1100 $cm^{-1}$ gap between them, similar to the spacing predicted here. As described by Kasha's rule, emission from $S_2$ is generally forbidden because of rapid


DOI: 10.1021/jacs.8b09149
J. Am. Chem. Soc. XXXX, XXX, XXX−XXX

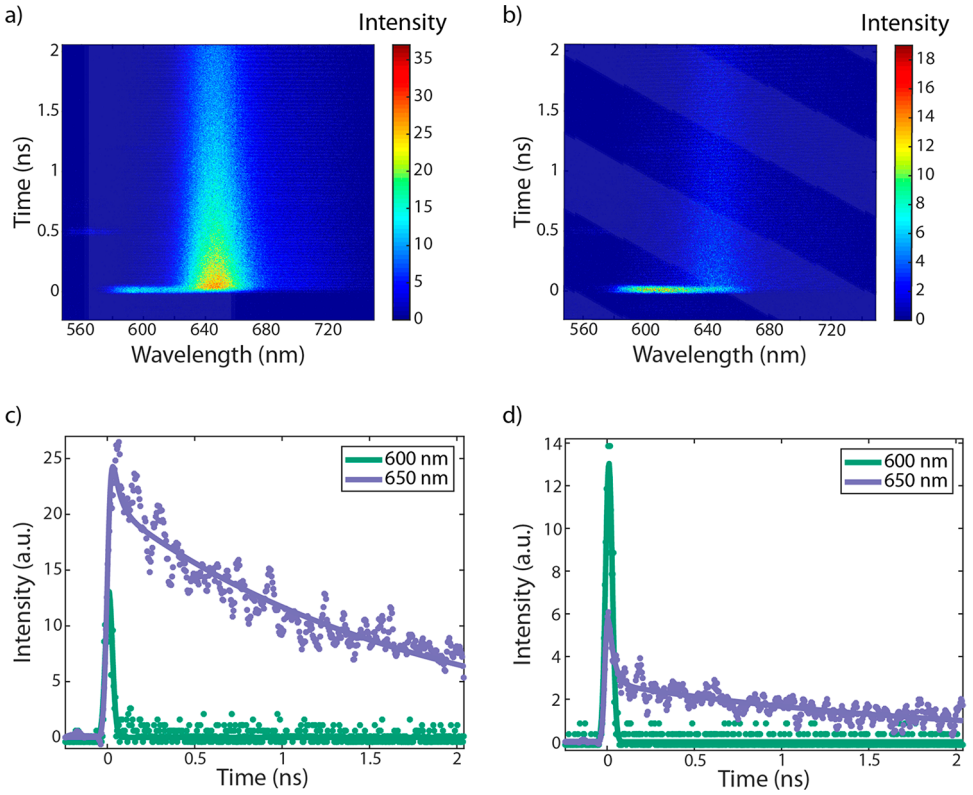


**Figure 17.** Time and wavelength-resolved emission of **monomer** nanoparticles before (a,c) and after (b,d) heating. In lifetime fits of unheated (c) and heated (d) **monomer** nanoparticles, the fluorescence of the blue satellite peak at 600 nm decays with a lifetime of <40 ps, limited by the instrument time resolution. The main peak at 650 nm fluorescence is well fit by a biexponential for both heated and unheated samples, with components of lifetime <40 ps and 2 ± 0.2 ns in the unheated sample (c) or 1.7 ± 0.2 ns in the heated sample (d). In the heated samples, the relative amplitude of the ultrafast decay increases significantly.

internal conversion, similar to emission from the upper exciton band. However, in species where the gap is large, radiative emission from $S_2$ not only competes with internal conversion to $S_1$, but can be the dominant decay channel.

We propose that the blue-shifted satellite peak is emission from the upper exciton state in a strongly coupled H-aggregate, Figure 16. We emphasize that the satellite peak is in most cases substantially less intense than the main peak, and thus emission from the species does not need to completely outcompete internal conversion, it just needs to be competitive enough to have a non-negligible quantum yield of emission. Thus, we expect the lifetime of this emissive species to be extremely short since internal conversion is still expected to be in the picosecond range. Bayda[64] also considered the possibility of this mechanism, but ultimately found a long-lived emission species, and thus rejected it in favor of thermal repopulation of the upper exciton-coupled state.

To test this prediction, **monomer** in 0.1% toluene/IPA was spin-coated on glass coverslips at 5 $\mu$g/mL to create an array of nanoparticles which were investigated via fluorescence lifetime spectroscopy using 560 nm pump light with 100 kHz repetition rate at 15 nJ/pulse. Emission was detected on a streak camera with 40 ps time resolution. As shown in Figure 17a,c, the main peak and blue satellite observed in the single-particle fluorescence spectra are visible in the lifetime spectra. The major peak at 650 nm has a 2 ns lifetime, typical of emission from an organic dye, but the emission from the blue satellite peak is extremely short-lived, with lifetime <40 ps, the streak camera time resolution. The extremely fast decay of the blue satellite fluorescence is consistent with emission from a higher electronic excited state like an upper exciton level, with an extremely short observed lifetime likely due to competition from a fast nonradiative decay. This short lifetime also additionally rules out emission from the bottom manifold of an H-aggregate via a softening of the symmetry rules forbidding emission, as described above, because this mechanism would be associated with a ns or greater lifetime. Spin-coated **monomer** nanoparticles heated at 80 °C for 3 h behaved similarly to photothermally heated samples that showed an increased intensity of the blue satellite peak, Figure 10. Here, preheated samples showed an increased intensity of the blue satellite from 4% to 19% of the main fluorescence peak, with a similarly instrument-limited measured lifetime, Figure 17b,c.

With this mechanism supported by time-resolved fluorescence, we can now present a succinct picture of how morphology maps onto emission properties. Computational results based on our crystal structure suggests domains ranging from the strongly H-coupled to the weakly J-coupled, Figure 15a. Species ranging from weakly H-coupled to strongly J-coupled should show emission in a spectral range near the isolated fluorophore and extending red, Figure 15b. Moderately H-coupled species should show no emission, as in these cases the internal conversion depopulating the upper exciton band is swift, as predicted by the energy gap law. Finally, strongly H-coupled species should show weak, short-lived blue-shifted emission, as observed. Finally, the presence of the quenched range at moderate H-coupling means that this blue-shifted emission would appear as an isolated peak, Figure 15c, as observed in Figure 8.


DOI: 10.1021/jacs.8b09149
J. Am. Chem. Soc. XXXX, XXX, XXX−XXX

It is likely that domains that display this characteristic blue emission are rather small. Even in optimally H-aggregated 1×*N* structures where *N* is large, Figure 14, though much of the density of states will be concentrated at the bottom of the energy ladder, some states will be distributed throughout the energy gap. These states may still provide efficient conduits for internal conversion, and as a consequence quenching, due to being closer in energy to the higher emissive states as predicted by the energy gap law. Alternatively, in large 1×*N* systems multiple closely spaced levels at the top of the manifold may be emissive, and consecutive relaxation through these levels may afford another pathway for emission, as the need to pass through multiple states could allow the slower radiative relaxation the opportunity to play a weak role. This pathway would also present with a fast excited state lifetime, as observed, and cannot be confirmed or ruled out with the available data.

While the computation in Figure 14 suggests a maximum blue shift of ∼900 $cm^{-1}$, some of the satellite peaks shown in Figure 8 are even more blueshifted from the isolated monomer. Two factors may contribute to this difference. First, the DFT calculations in Figure 14 involve transition densities, and may overestimate charge delocalization. On the other hand, computation with point dipoles (see SI) predicts larger shifts up to ∼1700 $cm^{-1}$, with the true value likely lying somewhere between these limiting cases. Second, as discussed above, the crystal structure in Figure 12 should not be taken as a direct representation as to the precise ordering present in the nanoparticles, and that likely a diversity of molecular packings exists. Reduction of the intraunit cell BODIPY−BODIPY distance by only 15% would elevate the blue shift to ∼1500 $cm^{-1}$ even via the transition density calculation.

**Understanding Spatially Nonuniform Particles, Particle Thermal Evolution, and Spectral Diffusion.** The scale in Figure 15 provides a framework to understand how the emissive properties of the nanoparticles vary in space and time, summarized in Figure 18. In the large particles in Figure 10, panel a) shows a spectral channel that includes the blue satellite peak, while panels b) and c) show a spectral channel that includes the red edge of the main peak. Just after deposition, upon excitation at 532 nm, considerably blue of the isolated monomer, the outer rims of the nanoparticles show evidence of the blue satellite peak. Excitation at 633 nm, resonant with the isolated monomer peak, results in only weak emission at the outer rim. Thus, the outer rim is composed predominantly of moderately and strongly coupled H-aggregates, resulting in domains that emit in the satellite peak or not at all. In contrast, the centers of the particles show emission in the main peak when excited at 532 or 633 nm. Thus, the centers are composed predominantly of domains that show weak H- or J-aggregation, with no evidence of the blue satellite and dominant emission in the red channel. These behavior are summarized in Figure 18a.

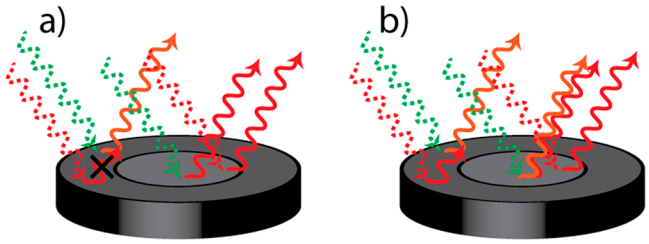


**Figure 18.** Model of spatially inhomogeneous particle emission properties with input (dashed) and output (solid) photons represented as wavy lines. Before photothermal annealing, (a) particle rims demonstrate orange (blue satellite) emission upon green excitation, and no emission upon red excitation, while particle centers demonstrate red emission regardless of whether green or red excitation is applied. In contrast, after photothermal annealing, (b) particle rims demonstrate orange (blue satellite) emission upon green excitation, and red emission upon red excitation, while particle centers demonstrate red emission with red excitation and both red and orange emission upon green excitation.

Upon exposure to prolonged 532 nm excitation, photobrightening occurs in both larger and smaller nanoparticles. After this process occures in the larger nanoparticles, the outer rim exhibits a more intense blue satellite when excited at 532 nm, and moderate red emission when excited at 633 nm. Simultaneously, the center shows more intense emission in the red channel when excited at 633 nm, but now shows both blue satellite and main peak emission when excited at 532 nm. The scale in Figure 15 can be used to understand this transition. These dynamics are consistent with Ostwald ripening-like behavior, whereby the size distribution of aggregates becomes more extreme over time, previously reported in the synthesis of one-dimensional organic nanorods.[66] Throughout the nanoparticle, midsized domains that likely fell in the quenched portion of Figure 15c are being photothermally annealed, resulting in rearrangement of dye molecules inside the particle into more small domains that are more strongly H-coupled, as well as more large domains that exhibit weak J- or weak H-coupling. Thus, the main and satellite peaks both become stronger, as observed.

Single-particle emission spectra of small particles show (Figure 8) that the appearance of the blue satellite peak is highly dynamic, with the feature blinking and undergoing spectral diffusion or even showing multiple peaks. This observation is consistent with the mechanism above, that photothermal annealing results in domain-shifting structural changes. As the domains change size, their degree of H-coupling changes, moving along the scale in Figure 15c, resulting in a peak that changes its spectral location and amplitude. This strong correlation between domain geometry and emission properties then manifests itself in small nanoparticles, where there may only be one strongly H-coupled domain that is emissive, allowing observation of blinking and spectral diffusion (Figure 8, orange trace). In larger particles, these dynamics are apparent as brightening and darkening in different spectral channels (Figure 10). In single-particle spectra, the role of irreversible photobleaching is also more conspicuous at later times.

**Alternative Theories for Blue Satellite Emission.** The observations described above are consistent with a mechanism where strongly coupled H-aggregates are capable of weakly emitting from the upper exciton band. Origins that rely on the presence of an impurity, a photochemical rearrangement, or emission from the lower manifold of states of the H-aggregate have all been ruled out above.

Another possibility is that rather than the blue satellite peak resulting from blue-shifted $S_1$ emission due to H-aggregation, it is red-shifted $S_2$ emission due to J-aggregation. This emission, accelerated over internal conversion due to the strong radiative rate enhancement associated with superluminescence,[67] would also manifest itself as a short-lived radiative state. However, we consider this mechanism unlikely, as the $S_2$ state has extremely


DOI: 10.1021/jacs.8b09149
J. Am. Chem. Soc. XXXX, XXX, XXX−XXX

small oscillator strength ($f$ = 0.006), and is blue-shifted from the $S_1$ state by over 3400 $cm^{-1}$ (Supporting Information), requiring an unphysically large degree of J-coupling in order to form the blue satellite peak.

Another potential explanation of the blue-shifted satellite peak is emission from a higher energy mode in the vibronic progression of the dye. Because the minor peak is blue of the major emission peak and the 0-0 transition of H-aggregates is suppressed,[52] it is tempting to assign the satellite to the 0-0 vibronic relaxation. However, emission in this manner would be expected to be commensurate with an excited state lifetime that is similar to or longer than that for the main emission peak, which is not observed.

A final possible explanation considers the role of thermal repopulation of the upper excited state, superficially similar to the phenomenon of thermally activated delayed fluorescence (TADF) where a singlet state is thermally repopulated from a lower lying triplet state.[68] However, gaps of ~1000 $cm^{-1}$ are considerably larger than kT (200 $cm^{-1}$) at room temperature. But, because excitation is made significantly blue-shifted of the absorption peak, a significant amount of local heating will occur, as described above as the origin of the observed photothermal annealing. Thus, immediately after excitation a substantial amount of thermal energy would be available for partially repopulating the upper state. The lifetime of the emission from the upper exciton band would also be limited by the lifetime of this excess thermal energy, predicting a very short excited state lifetime, as observed. This situation is distinct from what is typically observed in TADF or in Bayda's system.[64] In the limit of complete equilibration, smaller energy gaps would also be predicted to be susceptible to this scheme of upper state repopulation, as detailed balance would require that repopulation rate to rise as the rate of depopulation of the upper state, internal conversion, also rises. Because we do not observe emission from species with intermediate gaps, this mechanism can only be valid if full equilibration is not reached and detailed balance is not enforced, leaving smaller gap emissive units effectively nonemissive from the upper state because internal conversation is still too fast. With the available evidence, we cannot eliminate nonequilibrium thermal repopulation as a possible mechanism.

## CONCLUSIONS

When a bulky norbornyl alkyl tail is affixed to a spirofluorene-functionalized BODIPY, the resulting self-assembled nanoparticles contain quasi-two-dimensional sheets of chromophores that present a rich example of the complex relationship between structure and photophysical properties. The micromorphology of the domains, in particular the repetition of the unit cell along orthogonal axes, results in qualitatively different photophysical behavior, ranging from weak J-coupling to strong H-coupling. The strongest H-coupled domains have a blue satellite emission peak with picosecond excited-state lifetime consistent with the rare process of emission from the upper exciton level, a process forbidden by Kasha's rule but observable because of the strong H-coupling. Spectrally resolved imaging, time-resolved fluorescence spectroscopy, photothermal effects, and spectral diffusion at the single-particle level show that these domains are spatially inhomogeneous and temporally dynamic.

The theme of coupling between structure and properties is an important one in organic electronic materials. Here, the availability of a crystal structure, and an unusual coexistence of two extremely different photophysical phenomena, even in the same nanoparticle, allows the unique opportunity to directly map structure from a photophysical observable in an organic nanoparticle, and as that physical structure evolves in space and time, so too does the photophysical behavior. Further, this work demonstrates a striking example of how structural defects can alter emission profiles, with emission from strongly H-aggregated domains providing a potential path for reducing spectral purity, a necessary requirement for OLEDs. Continued efforts at mapping structure and optical properties will reveal more mechanisms for how certain motifs in electronic structure can yield desired properties, whereas others represent pitfalls to be avoided.

## ASSOCIATED CONTENT

### Supporting Information

The Supporting Information is available free of charge on the ACS Publications website at DOI: 10.1021/jacs.8b09149.

Additional experimental and computational details, synthesis, chemical, optical, and materials characterization (PDF)

Large monomer particles excited at 532 nm imaged in blue channel (AVI)

Large monomer particles excited at 532 nm imaged in red channel (AVI)

Large monomer particles excited at 640 nm imaged in red channel (AVI)

## AUTHOR INFORMATION


### Corresponding Author

*rhg@chem.wisc.edu

### ORCID

Stephen Lee: 0000-0003-2614-286X
Semion K. Saikin: 0000-0003-1924-3961
Michael R. Wasielewski: 0000-0003-2920-5440
Julie S. Biteen: 0000-0003-2038-6484
Padma Gopalan: 0000-0002-1955-640X
Randall H. Goldsmith: 0000-0001-9083-8592

### Author Contributions

‡These authors contributed equally.


### Notes

The authors declare no competing financial interest.

## ACKNOWLEDGMENTS

We are thankful to Dr. Bruce Noll (Bruker) for collecting single-crystal X-ray diffraction data and to Dr. Ilia A. Guzei (UW−Madison) for helpful structural discussions. We thank Prof. John Wright for discussions of photodynamics. We acknowledge support from the staff and the use of equipment at the Materials Science Center and Soft Materials equipment at the Materials Science Center at the University of Wisconsin-Madison. SKS is thankful to the Tata Sons Limited - Alliance Agreement (A32391) and also to the Ministry of Education and Science of the Russian Federation for supporting the research in the framework of the state assignment, award # 3.2166.2017/4.6. RHG acknowledges support from NSF CHE-1254936. JSB acknowledges support from NSF CHE-1807676. PG acknowledges partial support from the Division of Materials Sciences and Engineering, Office of Basic Energy Science, U.S. Department of Energy under Award No. ER46590 for characterization of these chromophores. PG



DOI: 10.1021/jacs.8b09149
J. Am. Chem. Soc. XXXX, XXX, XXX−XXX

and JS acknowledge partial support from the National Science Foundation- DMR-1507409. JS acknowledges support from the National Science Foundation- DMR-1507409 for X-ray diffraction studies. MRW acknowledges support from the U.S. Department of Energy, Office of Science, Office of Basic Energy Sciences under Award DE-FG02−99ER14999 for time-resolved fluorescence measurements. This material is based upon work supported by the National Science Foundation Graduate Research Fellowship under Grant No. DGE-1256259 (to DAH).

## REFERENCES

(1) Haedler, A. T.; Kreger, K.; Issac, A.; Wittmann, B.; Kivala, M.; Hammer, N.; Köhler, J.; Schmidt, H.-W.; Hildner, R. Long-Range Energy Transport in Single Supramolecular Nanofibres at Room Temperature. *Nature* **2015**, *523*, 196−200.

(2) Caram, J. R.; Doria, S.; Eisele, D. M.; Freyria, F. S.; Sinclair, T. S.; Rebentrost, P.; Lloyd, S.; Bawendi, M. G. Room-Temperature Micron-Scale Exciton Migration in a Stabilized Emissive Molecular Aggregate. *Nano Lett.* **2016**, *16*, 6808−6815.

(3) Spano, F. C.; Mukamel, S. Superradiance in Molecular Aggregates. *J. Chem. Phys.* **1989**, *91*, 683−700.

(4) Upadhyay, S. P.; Lupo, K. M.; Marquard, A. N.; Ng, J. D.; Bates, D. M.; Goldsmith, R. H. Fluorescent Dendrimeric Molecular Catalysts Demonstrate Unusual Scaling Behavior at the Single-Molecule Level. *J. Phys. Chem. C* **2015**, *119*, 19703−19714.

(5) Hofkens, J.; Maus, M.; Gensch, T.; Vosch, T.; Cotlet, M.; Köhn, F.; Herrmann, A.; Müllen, K.; De Schryver, F. Probing Photophysical Processes in Individual Multichromophoric Dendrimers by Single-Molecule Spectroscopy. *J. Am. Chem. Soc.* **2000**, *122*, 9278−9288.

(6) Cotlet, M.; Gronheid, R.; Habuchi, S.; Stefan, A.; Barbafina, A.; Müllen, K.; Hofkens, J.; De Schryver, F. C. Intramolecular Directional Förster Resonance Energy Transfer at the Single-Molecule Level in a Dendritic System. *J. Am. Chem. Soc.* **2003**, *125*, 13609−13617.

(7) Wasielewski, M. R. Self-Assembly Strategies for Integrating Light Harvesting and Charge Separation in Artificial Photosynthetic Systems. *Acc. Chem. Res.* **2009**, *42*, 1910−1921.

(8) Liess, A.; Lv, A.; Arjona-Esteban, A.; Bialas, D.; Krause, A.-M.; Stepanenko, V.; Stolte, M.; Würthner, F. Exciton Coupling of Merocyanine Dyes from H- to J-Type in the Solid State by Crystal Engineering. *Nano Lett.* **2017**, *17*, 1719−1726.

(9) Wu, H.; Xue, L.; Shi, Y.; Chen, Y.; Li, X. Organogels Based on J- and H-Type Aggregates of Amphiphilic Perylenetetracarboxylic Diimides. *Langmuir* **2011**, *27*, 3074−3082.

(10) Turro, N. J.; Ramamurthy, V.; Scaiano, J. C. *Principles of Molecular Photochemistry*; University Science Books: Sausalito, CA, 2009.

(11) Peng, H.-S.; Chiu, D. T. Soft Fluorescent Nanomaterials for Biological and Biomedical Imaging. *Chem. Soc. Rev.* **2015**, *44*, 4699−4722.

(12) Wu, C.; Jin, Y.; Schneider, T.; Burnham, D. R.; Smith, P. B.; Chiu, D. T. Ultrabright and Bioorthogonal Labeling of Cellular Targets Using Semiconducting Polymer Dots and Click Chemistry. *Angew. Chem., Int. Ed.* **2010**, *49*, 9436−9440.

(13) O'Neill, M.; Kelly, S. M. Ordered Materials for Organic Electronics and Photonics. *Adv. Mater.* **2011**, *23*, 566−584.

(14) Babu, S. S.; Prasanthkumar, S.; Ajayaghosh, A. Self-Assembled Gelators for Organic Electronics. *Angew. Chem., Int. Ed.* **2012**, *51*, 1766−1776.

(15) Morseth, Z. A.; Wang, L.; Puodziukynaite, E.; Leem, G.; Gilligan, A. T.; Meyer, T. J.; Schanze, K. S.; Reynolds, J. R.; Papanikolas, J. M. Ultrafast Dynamics in Multifunctional Ru(II)-Loaded Polymers for Solar Energy Conversion. *Acc. Chem. Res.* **2015**, *48*, 818−827.

(16) Schwartz, E.; Le Gac, S.; Cornelissen, J. J. L. M.; Nolte, R. J. M.; Rowan, A. E. Macromolecular Multi-Chromophoric Scaffolding. *Chem. Soc. Rev.* **2010**, *39*.1576

(17) Trenor, S. R.; Shultz, A. R.; Love, B. J.; Long, T. E. Coumarins in Polymers: From Light Harvesting to Photo-Cross-Linkable Tissue Scaffolds. *Chem. Rev.* **2004**, *104*, 3059−3077.

(18) Rong, Y.; Wu, C.; Yu, J.; Zhang, X.; Ye, F.; Zeigler, M.; Gallina, M. E.; Wu, I. C.; Zhang, Y.; Chan, Y.-H.; Sun, W.; Uvdal, K.; Chiu, D. T. Multicolor Fluorescent Semiconducting Polymer Dots with Narrow Emissions and High Brightness. *ACS Nano* **2013**, *7*, 376−384.

(19) Alemdaroglu, F. E.; Alexander, S. C.; Ji, D.; Prusty, D. K.; Börsch, M.; Herrmann, A. Poly(BODIPY)s: A New Class of Tunable Polymeric Dyes. *Macromolecules* **2009**, *42*, 6529−6536.

(20) Nagai, A.; Chujo, Y. Aromatic Ring-Fused BODIPY-Based Conjugated Polymers Exhibiting Narrow near-Infrared Emission Bands. *Macromolecules* **2010**, *43*, 193−200.

(21) Thivierge, C.; Loudet, A.; Burgess, K. Brilliant BODIPY-Fluorene Copolymers with Dispersed Absorption and Emission Maxima. *Macromolecules* **2011**, *44*, 4012−4015.

(22) Peterson, J. J.; Krauss, T. D. Photobrightening and Photodarkening in PbS Quantum Dots. *Phys. Chem. Chem. Phys.* **2006**, *8*, 3851−3856.

(23) Tice, D. B.; Frederick, M. T.; Chang, R. P. H.; Weiss, E. A. Electron Migration Limits the Rate of Photobrightening in Thin Films of CdSe Quantum Dots in a Dry $N_2$(g) Atmosphere. *J. Phys. Chem. C* **2011**, *115*, 3654−3662.

(24) Kowada, T.; Yamaguchi, S.; Ohe, K. Highly Fluorescent BODIPY Dyes Modulated with Spirofluorene Moieties. *Org. Lett.* **2010**, *12*, 296−299.

(25) Lupo, K. M.; Hinton, D. A.; Ng, J. D.; Padilla, N. A.; Goldsmith, R. H. Probing Heterogeneity and Bonding at Silica Surfaces through Single-Molecule Investigation of Base-Mediated Linkage Failure. *Langmuir* **2016**, *32*, 9171−9179.

(26) Ng, J. D.; Upadhyay, S. P.; Marquard, A. N.; Lupo, K. M.; Hinton, D. A.; Padilla, N. A.; Bates, D. M.; Goldsmith, R. H. Single-Molecule Investigation of Initiation Dynamics of an Organometallic Catalyst. *J. Am. Chem. Soc.* **2016**, *138*, 3876−3883.

(27) Banal, J. L.; White, J. M.; Ghiggino, K. P.; Wong, W. W. H. Concentrating Aggregation-Induced Fluorescence in Planar Waveguides: A Proof-of-Principle. *Sci. Rep.* **2015**, *4*, 1−5.

(28) Choi, T.-L.; Grubbs, R. H. Controlled Living Ring-Opening-Metathesis Polymerization by a Fast-Initiating Ruthenium Catalyst. *Angew. Chem., Int. Ed.* **2003**, *42*, 1743−1746.

(29) Loudet, A.; Burgess, K. BODIPY Dyes and Their Derivatives: Syntheses and Spectroscopic Properties. *Chem. Rev.* **2007**, *107*, 4891−4932.

(30) Ulrich, G.; Ziessel, R.; Harriman, A. The Chemistry of Fluorescent BODIPY Dyes: Versatility Unsurpassed. *Angew. Chem., Int. Ed.* **2008**, *47*, 1184−1201.

(31) Parry, A. V. S.; Lu, K.; Tate, D. J.; Urasinska-Wojcik, B.; Caras-Quintero, D.; Majewski, L. A.; Turner, M. L. Trichlorosilanes as Anchoring Groups for Phenylene-Thiophene Molecular Monolayer Field Effect Transistors. *Adv. Funct. Mater.* **2014**, *24*, 6677−6683.

(32) Horak, E. H.; Rea, M. T.; Heylman, K. D.; Gelbwaser-Klimovsky, D.; Saikin, S. K.; Thompson, B. J.; Kohler, D. D.; Knapper, K. A.; Wei, W.; Pan, F.; Gopalan, P.; Wright, J. C.; Aspuru-Guzik, A.; Goldsmith, R. H. Exploring Electronic Structure and Order in Polymers Via Single-Particle Microresonator Spectroscopy. *Nano Lett.* **2018**, *18*, 1600−1607.

(33) Vogelsang, J.; Adachi, T.; Brazard, J.; Vanden Bout, D. A.; Barbara, P. F. Self-Assembly of Highly Ordered Conjugated Polymer Aggregates with Long-Range Energy Transfer. *Nat. Mater.* **2011**, *10*, 942−946.

(34) Bolinger, J. C.; Traub, M. C.; Brazard, J.; Adachi, T.; Barbara, P. F.; Vanden Bout, D. A. Conformation and Energy Transfer in Single Conjugated Polymers. *Acc. Chem. Res.* **2012**, *45*, 1992−2001.

(35) Vogelsang, J.; Lupton, J. M. Solvent Vapor Annealing of Single Conjugated Polymer Chains: Building Organic Optoelectronic Materials from the Bottom Up. *J. Phys. Chem. Lett.* **2012**, *3*, 1503−1513.



DOI: 10.1021/jacs.8b09149
J. Am. Chem. Soc. XXXX, XXX, XXX−XXX

(36) Weston, K. D.; Dyck, M.; Tinnefeld, P.; Müller, C.; Herten, D. P.; Sauer, M. Measuring the Number of Independent Emitters in Single-Molecule Fluorescence Images and Trajectories Using Coincident Photons. *Anal. Chem.* **2002**, *74*, 5342−5349.
(37) De Schryver, F. C.; Vosch, T.; Cotlet, M.; Van der Auweraer, M.; Müllen, K.; Hofkens, J. Energy Dissipation in Multichromophoric Single Dendrimers. *Acc. Chem. Res.* **2005**, *38*, 514−522.
(38) Yang, J.; Cho, S.; Yoo, H.; Park, J.; Li, W.-S.; Aida, T.; Kim, D. Control of Molecular Structures and Photophysical Properties of Zinc(II) Porphyrin Dendrimers Using Bidentate Guests: Utilization of Flexible Dendrimer Structures as a Controllable Mold. *J. Phys. Chem. A* **2008**, *112*, 6869−6876.
(39) Noriega, R.; Barnard, E. S.; Ursprung, B.; Cotts, B. L.; Penwell, S. B.; Schuck, P. J.; Ginsberg, N. S. Uncovering Single-Molecule Photophysical Heterogeneity of Bright, Thermally Activated Delayed Fluorescence Emitters Dispersed in Glassy Hosts. *J. Am. Chem. Soc.* **2016**, *138*, 13551−13560.
(40) Yoo, H.; Yang, J.; Yousef, A.; Wasielewski, M. R.; Kim, D. Excimer Formation Dynamics of Intramolecular Π-Stacked Perylenediimides Probed by Single-Molecule Fluorescence Spectroscopy. *J. Am. Chem. Soc.* **2010**, *132*, 3939−3944.
(41) Huser, T.; Yan, M.; Rothberg, L. J. Single Chain Spectroscopy of Conformational Dependence of Conjugated Polymer Photophysics. *Proc. Natl. Acad. Sci. U. S. A.* **2000**, *97*, 11187−11191.
(42) Ebihara, Y.; Vacha, M. Relating Conformation and Photophysics in Single Meh-Ppv Chains. *J. Phys. Chem. B* **2008**, *112*, 12575−12578.
(43) Barbara, P. F.; Gesquiere, A. J.; Park, S.-J.; Lee, Y. J. Single-Molecule Spectroscopy of Conjugated Polymers. *Acc. Chem. Res.* **2005**, *38*, 602−610.
(44) Van Munster, E. B.; Kremers, G. J.; Adjobo-Hermans, M. J. W.; Gadella, T. W. J., Jr Fluorescence Resonance Energy Transfer (FRET) Measurement by Gradual Acceptor Photobleaching. *J. Microsc.* **2005**, *218*, 253−262.
(45) Wang, X.; Groff, L. C.; McNeill, J. D. Photoactivation and Saturated Emission in Blended Conjugated Polymer Nanoparticles. *Langmuir* **2013**, *29*, 13925−13931.
(46) Huisgen, R.; Ooms, P. H. J.; Mingin, M.; Allinger, N. L. Exceptional Reactivity of the Bicyclo[2.2.1]Heptene Double Bond. *J. Am. Chem. Soc.* **1980**, *102*, 3951−3953.
(47) Rondan, N. G.; Paddon-Row, M. N.; Caramella, P.; Mareda, J.; Mueller, P. H.; Houk, K. N. Origin of Huisgen's Factor "X": Staggering of Allylic Bonds Promotes Anomalously Rapid Exo Attack on Norbornenes. *J. Am. Chem. Soc.* **1982**, *104*, 4974−4976.
(48) Braun, M.; Christl, M.; Peters, E.-M.; Peters, K. Photochemical Reactions of Chloranil with Norbornene,† Bicyclo[2.1.1]Hex-2-Ene and Cyclopentene. A Novel Intermolecular Photocycloaddition. *J. Chem. Soc., Perkin Trans. 1* **1999**, *1*, 2813−2820.
(49) Saikin, S. K.; Eisfeld, A.; Valleau, S.; Aspuru-Guzik, A. Photonics Meets Excitonics: Natural and Artificial Molecular Aggregates. *Nanophotonics* **2013**, *2*, 21−38.
(50) Saikin, S. K.; Shakirov, M. A.; Kreisbeck, C.; Peskin, U.; Proshin, Y. N.; Aspuru-Guzik, A. On the Long-Range Exciton Transport in Molecular Systems: The Application to H-Aggregated Heterotriangulene Chains. *J. Phys. Chem. C* **2017**, *121*, 24994−25002.
(51) Spano, F. C. The Spectral Signatures of Frenkel Polarons in H- and J-Aggregates. *Acc. Chem. Res.* **2010**, *43*, 429−439.
(52) Spano, F. C.; Silva, C. H- and J-Aggregate Behavior in Polymeric Semiconductors. *Annu. Rev. Phys. Chem.* **2014**, *65*, 477−500.
(53) Panzer, F.; Sommer, M.; Bässler, H.; Thelakkat, M.; Köhler, A. Spectroscopic Signature of Two Distinct H-Aggregate Species in Poly(3-Hexylthiophene). *Macromolecules* **2015**, *48*, 1543−1553.
(54) Clark, J.; Silva, C.; Friend, R. H.; Spano, F. C. Role of Intermolecular Coupling in the Photophysics of Disordered Organic Semiconductors: Aggregate Emission in Regioregular Polythiophene. *Phys. Rev. Lett.* **2007**, *98*, No. 206406, DOI: 10.1103/PhysRevLett.98.206406.
(55) Rösch, U.; Yao, S.; Wortmann, R.; Würthner, F. Fluorescent H-Aggregates of Merocyanine Dyes. *Angew. Chem.* **2006**, *118*, 7184−7188.
(56) Peyratout, C.; Daehne, L. Aggregation of Thiacyanine Derivatives on Polyelectrolytes. *Phys. Chem. Chem. Phys.* **2002**, *4*, 3032−3039.
(57) Chakraborty, S.; Debnath, P.; Dey, D.; Bhattacharjee, D.; Hussain, S. A. Formation of Fluorescent H-Aggregates of a Cyanine Dye in Ultrathin Film and Its Effect on Energy Transfer. *J. Photochem. Photobiol., A* **2014**, *293*, 57−64.
(58) Chaudhuri, D.; Li, D.; Che, Y.; Shafran, E.; Gerton, J. M.; Zang, L.; Lupton, J. M. Enhancing Long-Range Exciton Guiding in Molecular Nanowires by H-Aggregation Lifetime Engineering. *Nano Lett.* **2011**, *11*, 488−492.
(59) Margulies, E. A.; Shoer, L. E.; Eaton, S. W.; Wasielewski, M. R. Excimer Formation in Cofacial and Slip-Stacked Perylene-3,4:9,10-Bis(Dicarboximide) Dimers on a Redox-Inactive Triptycene Scaffold. *Phys. Chem. Chem. Phys.* **2014**, *16*, 23735−23742.
(60) Mandal, A. K.; Pal, M. K. Strong Fluorescence Emissions by H-Aggregates of the Dye Thiacyanine in the Presence of the Surfactant Aerosol-OT. *Chem. Phys.* **2000**, *253*, 115−124.
(61) Hirose, T.; Tsunoi, Y.; Fujimori, Y.; Matsuda, K. Fluorescence Enhancement of Covalently Linked 1-Cyano-1,2-Diphenylethene Chromophores with Naphthalene-1,8-Diyl Linker Units: Analysis Based on Kinetic Constants. *Chem. - Eur. J.* **2015**, *21*, 1637−1644.
(62) Verma, P.; Pal, H. Intriguing H-Aggregate and H-Dimer Formation of Coumarin-481 Dye in Aqueous Solution as Evidenced from Photophysical Studies. *J. Phys. Chem. A* **2012**, *116*, 4473−4484.
(63) Qian, H.; Cousins, M. E.; Horak, E. H.; Wakefield, A.; Liptak, M. D.; Aprahamian, I. Suppression of Kasha's Rule as a Mechanism for Fluorescent Molecular Rotors and Aggregation-Induced Emission. *Nat. Chem.* **2017**, *9*, 83−87.
(64) Bayda, M.; Dumoulin, F.; Hug, G. L.; Koput, J.; Gorniak, R.; Wojcik, A. Fluorescent H-Aggregates of an Asymmetrically Substituted Mono-Amino Zn(II) Phthalocyanine. *Dalton Trans.* **2017**, *46*, 1914−1926.
(65) Itoh, T. Fluorescence and Phosphorescence from Higher Excited States of Organic Molecules. *Chem. Rev.* **2012**, *112*, 4541−4568.
(66) Mahesh, S.; Gopal, A.; Thirumalai, R.; Ajayaghosh, A. Light-Induced Ostwald Ripening of Organic Nanodots to Rods. *J. Am. Chem. Soc.* **2012**, *134*, 7227−7230.
(67) Lim, S. H.; Bjorklund, T. G.; Spano, F. C.; Bardeen, C. J. Exciton Delocalization and Superradiance in Tetracene Thin Films and Nanoaggregates. *Phys. Rev. Lett.* **2004**, *92*, No. 107402, DOI: 10.1103/PhysRevLett.92.107402.
(68) Yang, Z.; Mao, Z.; Xie, Z.; Zhang, Y.; Liu, S.; Zhao, J.; Xu, J.; Chi, Z.; Aldred, M. P. Recent Advances in Organic Thermally Activated Delayed Fluorescence Materials. *Chem. Soc. Rev.* **2017**, *46*, 915−1016.


DOI: 10.1021/jacs.8b09149
J. Am. Chem. Soc. XXXX, XXX, XXX−XXX